Characterisation of Received Signal Strength Perturbations using Allan Variance

Chunbo Luo[†], Pablo Casaseca-de-la-Higuera[‡], Sally McClean[%], Gerard Parr[◇], Peng Ren[$]

† College of Engineering, Mathematics and Physical Sciences, University of Exeter, Exeter, EX4 4QF, UK
‡ School of Engineering and Computing, University of the West of Scotland, Paisley, PA1 2BE, UK
% School of Computing and Information Engineering, University of Ulster, Coleraine, BT52 1SA, UK.
◇ School of Computing Sciences, University of East Anglia, Norwich, NR4 7TJ, UK
$ China University of Petroleum(Huadong), Qingdao 266580, China.
E-mail: c.luo@exeter.ac.uk, pablo.casaseca@uws.ac.uk,
si.mcclean@ulster.ac.uk, G.Parr@uea.ac.uk, pengren@upc.edu.cn

Abstract—The received signal strength (RSS) of wireless signals conveys important information that has been widely used in wireless communications, localisation and tracking. Traditional RSS-based research and applications model the RSS signal using a deterministic component plus a white noise term. This paper investigates the assumption of white noise to have a further understanding of the RSS signal and proposes a methodology based on the Allan Variance (AVAR) to characterise it. Using AVAR, we model the RSS unknown perturbations as correlated random terms. These terms can account for both coloured noise or other effects such as shadowing or small-scale fading. Our results confirm that AVAR can be used to obtain a flexible model of the RSS perturbations, as expressed by coloured noise components . The study is complemented by introducing two straightforward applications of the proposed methodology: 1) The modelling and simulation of RSS noise using Wiener processes, and 2) RSS localisation using the extended Kalman filter.

Index Terms—Received Signal Strength (RSS), coloured noise, Allan variance, Kalman filter, RSS simulation, RSS based localization

I. INTRODUCTION

Wireless signals are widely used for data and voice communications, object detection and localization. These systems (e.g. wireless sensor networks) often utilize the received signal strength (RSS) as a performance index because its value indicates the signal quality and suggests whether the system can properly function or not [1]–[6]. Such applications can be found in mobile sensor networks and robotic cooperative networks where RSS is used to estimate the position of each node. It is thus of great interest and practical importance to measure and model RSS as accurately as possible. For example, a node with inaccurate RSS may lead to failure in detecting objects, cause communication outages between the source and destination, and provide inaccurate position information. Because of the dynamic propagation features of radio frequency channels and transceivers' electronic system noise, RSS measurements vary irregularly in practical scenarios, making their accurate identification and modelling not only an important task but also a difficult one.

The Friis transmission equation can be used to characterise and model the received wireless signal strength under ideal conditions of free space [7]. However, the practical propagation environment where wireless signals are generated and propagated is usually far from ideal due to reflection, scattering, diffraction, and attenuation. The dominating mechanism is influenced by a number of factors such as properties of the transmitted signal, interaction with surrounding objects, and relative movement of the receiver with respect to the transmitter [8]. In [9], the authors extensively studied the radio propagation channels and identified the reflecting surface, terrain type and fading as the three major factors which affect RSS values. The electronic systems and antennas equipped by the transmitter and receiver also contribute significantly to RSS measurements [10], [11].

It is thus necessary to properly characterise the perturbations present in RSS measurements so that their malignant effects can be reduced in practice. Since the distribution and second order statistics of these perturbations strongly depend on the propagation mechanisms, so far proposed models are typically constrained to specific propagation phenomena and do not allow considering multiple fading driving causes [12]. Thus, there is need of flexible models to characterise RSS perturbations allowing accurate estimation of the power spectral density (PSD) regardless the dominating propagation mechanism. Besides, to the best of our knowledge, the characterisation of coloured noise components in nonfaded RSS measurements has not been systematically studied so far [2], [5], [13]–[15]. The use of the aforementioned flexible models would allow further insight on the temporal changes of RSS signals.

A. Motivations from an Engineering perspective

A considerable effort has been devoted to the characterisation of wireless channels to enable successful deployment of communication systems. This covers a span ranging from the classic work by Gudmundson [16], who proposed a simple decreasing correlation model for shadow fading outdoor radio channels, to more recent contributions such as [17] considering correlation in indoor channels due to both multipath reflections and shadowing, and the processing of phase noise using pulse Doppler processing algorithms and sidelobe blanker techniques [18].

The following factors can affect RSS in a practical wireless system:
1) Large scale path loss due to the distance travelled between transmitter and receiver.
2) Medium scale fading or shadowing: the effect of large objects in the channel in between transmitter and receiver.
3) Small scale fading: the effect of the constructive or destructive addition of multipath waves at the receiver as it moves on the order of a wavelength.
4) Temporal fading, due to the movement of people and objects in the environment.
5) Interference, due to the transmission of other signals in the same band.
6) Thermal noise.
7) Changes in transmit power, due to battery, temperature, or other changes in the transmitter hardware.

8) Changes in the RSS measuring circuit in the receiver, again, due to battery, temperature, or other changes in the receiver hardware.

The first three are static when the environment is unchanged, and the transmitter and receiver are stationary. Factors 4–8 may contribute to dynamic changes in measured RSS even in stationary conditions. Because of the complexity of identifying every affecting mechanism, a simplified treatment of RSS measurements with uncorrelated lognormal distributed perturbations[1] is widely accepted in the literature and usually applied in practical systems [8], [19], [20]. Specifically, RSS is modelled using four major terms: antenna gains, transmitting power, free space path loss and lognormal white noise. This can be used to model any uncertainty with a random term, which may include more effects than actual thermal noise[2]. Such assumptions offer a simple model to describe RSS and make its mathematical expression tractable. However, they can only be made if the noise PSD approximately spreads evenly over the whole bandwidth. If meaningful variations in the PSD do exist, the perturbations can no longer be considered as uncorrelated and this issue needs to be considered.

Considering the nature of wireless channels, modelling RSS perturbations as uncorrelated random processes does not seem sensible from the Engineering perspective. Instead, considering a correlated stochastic process accounting for unknown perturbations due to shadowing, reflections or any other temporal fading mechanism seems more reasonable. Furthermore, even in situations where the existence of temporal fading could be negligible, considering correlated perturbations might be advisable. For example, the measurements from some physical instruments present such noise components with both short and long term correlations due to circuit drifts leading to nonuniform spectral distributions [21]. Stebler *et al.* [22] state that in the spectral domain, if the measurement sensors such as the accelerometers and gyroscopes are corrupted by random errors of complex spectral structure, the methods such as AVAR or PSD analysis may fail due to the difficulty of separating the error processes. It is thus particular important to check if such problem exists in RSS measurements.

AVAR presents following advantages with respect to other methods for characterization of coloured noise: 1) AVAR is independent of the long-term systematic components in the investigated time series; 2) AVAR converges for most of the commonly encountered types of noise, whereas other classical methods do not always converge to a finite value; 3) In practical applications, it has weak sensitivity to low-frequency signal variations; 4) AVAR is more computationally effective than classical spectral methods and widely used to investigate the spectral characteristics of a time series for noise type identification [23].

B. Contributions

In this paper, we deal with the characterisation of correlated perturbations in RSS. We first demonstrate the time and system-dependency of noise in RSS measurements from practical system setups where no temporal fading is expected. As an effective and flexible instrument to analyse correlated stochastic processes, the AVAR is then introduced with a specific focus on its calculation [24]. The characterisation of RSS perturbations is thus performed using AVAR. A number of experiments considering different propagation setups are conducted and analysed. Based on these results, we further introduce two applications of the proposed

[1]We will use the word perturbation to refer to any unwanted signal term in the RSS measurements, regardless of its nature or driving mechanism.

[2]Without loss of generality, we refer to random perturbation as noise.

characterisation: 1) modelling coloured noise components using Gaussian Wiener processes and; 2) distance estimation from RSS measurements using an extended Kalman filter.

The main contribution of the paper is the proposal of a general approach to characterize the perturbations of RSS measurements, which can be applied to heterogeneous devices and different propagation environments. The first application is presented as a tool to develop further studies on positioning or channel estimation. Finally, we illustrate the application of this methodology, using distance estimation as a case study.

The remainder of the paper is as follows: Section II introduces the related work and background, and motivates the paper; Section III discusses RSS through the path loss model, the calculation of AVAR and perturbation model; Section IV presents different experiments using different setups; Section V presents the applications of modelling coloured noise using simulation and the extended Kalman filter (EKF) for RSS distance estimation; Section VI discusses the relevant issues of RSS measurements and modelling of perturbations, and Section VII concludes this paper.

II. RELATED WORK

A. RSS-based Research and Applications

RSS-based research and applications can be found in broad areas. One particular example is wireless communication, which requires an adequate level of RSS in order to establish connections or continue communications [8]. Parsons further investigated mobile radio propagation channels, and demonstrated that a propagation channel can affect the RSS by means of fading and noise and thus have strong impact towards the performance of a radio system [9]. Not only communication systems rely on accurate RSS measurement and modelling, but another large group of applications has also extensively exploited RSS, namely localization and tracking [3], [25]. Li *et al.* proposed to use RSS-based localization algorithms using LS channel estimation when the propagation model is unknown. In order to improve the accuracy of RSS based localization, Chandrasekaran *et al.* exploited the correlations in positioning errors over time. Practical application of RSS measurements was demonstrated in [1], [26], which implemented positioning and collision avoidance algorithms in unmanned aerial vehicle networks.

With an increasing interest on RSS-based applications, it becomes obvious that existing solutions supported by relatively unsophisticated techniques need to be further investigated, in order to have a better understanding of RSS perturbations, improve their modelling and enhance performance. The accuracy of using RSS-based localization is analyzed in [5], which shows that, in a cellular network, RSS-based localization has limited accuracy that does not meet specific government requirements, but is still an attractive solution for less demanding services. Arora and McGuire studied the lower bound of the localization estimation error of mobile terminals used in urban areas and suggested that the presence of buildings invalidates some popular assumptions for estimation errors such as the Cramer-Rao lower bound [27].

Our recent project [28] investigated the application of RSS measurements for the purpose of collision avoidance in unmanned aerial vehicle networks. We discovered that coloured noise can affect the algorithms at a certain level of accuracy, which has significance for such high mobility scenarios. This motivated us to explore the characteristics of RSS perturbations into greater details and model and simulate coloured noise for reconstruction and test purposes.

B. RSS Measurements Signal Model

Since RSS is an important feature of wireless signals, its modelling has been extensively studied. The Friis transmission equation [7] firstly introduced the free space propagation model. However, practical wireless systems and their applied environments are far from this ideal environment: the transmit and measurement circuits may drift with time and the propagation channels may randomly reflect or scatter signals and create fading. These radio propagation properties were studied and several path loss models (e.g. [29], [30]) were proposed and generalized as follows,

$$PL = \overline{PL} + X_\sigma \qquad (1)$$

where $\overline{PL}$ is the mean propagation loss and X_σ is a random variable accounting for any perturbation in the signal. This model error can include any unknown effect due to shadowing, multipath reflections, etc. When no fading is present, a model considering X_σ as a zero mean Gaussian distributed random variable with standard deviation σ is widely studied and accepted in the literature. The corresponding nonlogarithmic model assumes a lognormal distribution for the random term in natural units. Thus, if X_σ is described in the log domain, it will follow a Gaussian distribution. When fading is present, the data may follow Rayleigh, Rice, Weibull, or Gamma distributions depending on the dominating propagation mechanism [8]–[10].

C. White and Coloured Noise

The study of particle movements under thermal fluctuations [31] helped define and model noise. The approximation that the random forces – which control the particle movement – are uncorrelated as perceived by the particle itself is usually assumed. The movement driven by these random forces is called white noise. This concept was applied in the systems where, compared with its own time scale, the outside forces are under much shorter correlation times. Similar approximations can be found in physics and electronics [11], [32], etc.

However, when the time scale of such a process is comparable to the characteristic relaxation time of the system itself, any results obtained from white noise theory that make predictions about the dynamics do not lie within its regime of validity [21]. For example, the study of laser gyro systems dynamics has revealed the following noise components: quantization noise, instability bias etc. [33]. These noise types have comparable correlation time scales with regard to the gyro system itself.

Let us consider the random term in eq. (1). When no fading is present, this term is usually assumed as uncorrelated (white) noise whereas when any temporal fading exists, the perturbations are actually correlated, and this assumption can no longer be made. Even in cases where the assumption of white noise could be maintained, there might be some uncontrolled effects giving rise to noise components with correlation time scales comparable to the measurement instrument itself. In this case, the correlation of the random signal would not be negligible, and a further look on the different noise components seems advisable. In order to have a better understanding of RSS values, it is worthwhile having a flexible tool able to characterise correlated (coloured) noise without needing to know precisely the propagation mechanisms.

III. ANALYSIS OF RSS PERTURBATIONS

A. RSS and Time Dependency

A wireless system generates signals using its internal circuit and transmits them from its antennas. The radio frequency signals are broadcast through propagation media using electromagnetic waves. The major causes of the degradation of the received signal strength include thermal noise, antenna features and channel propagation loss. According to [10, equation (3.93)], the received signal strength can be given by

$$P_y(d)[dB] = P_x - \overline{PL}(d_0) - 10n \log(\frac{d}{d_0}) + X_\sigma \qquad (2)$$

where n is the path loss factor whose value is associated with the propagation environment [8], P_x is the transmitting power, d and d_0 are the transmitter-receiver distance and reference distance respectively. As described before, X_σ is the random perturbation (noise) term. The key symbols used in this paper are listed in Table I. Given a fixed position of transmitter and receiver, we can rewrite (2) to describe the time varying relationship as

$$P_y(t)[dB] = P_x - \overline{PL}(d_0) - 10n \log(\frac{d}{d_0}) + X_\sigma(t), \quad (3)$$

where the first three terms on the right hand side are not time varying.

When no fading is present, $X_\sigma(t)$ is usually modelled as a zero-mean Gaussian distributed random variable with standard deviation σ and PSD given by

$$S_w(f) = \frac{N_0}{2}$$

where $N_0 = 2\sigma^2$.

Using a white process to model the random variable is convenient in describing its movements driven by random forces and has the advantage of simplicity in the mathematical expression and analysis. However, it can be an over simplification for describing practical systems where the noise is from complicated sources and shows different behaviours at different correlation times [33]. In order to verify that the noise present in RSS measurements is actually coloured, we tested a dataset of $N = 15000$ Line of Sight (LOS) RSS measurements[3] from an 802.11g receiver against the null hypothesis of whiteness of the noise. We employed the Ljung-Box Q-test [34] for the sample autocorrelation coefficient of the noise process $X_\sigma(j), j = 1, \ldots, N$:

$$\hat{\rho}(k) = \frac{\sum_{j=k+1}^{N} X_\sigma(j)X_\sigma(j-k)}{\sum_{j=1}^{N} X_\sigma^2(j)} \quad k \in \mathbb{Z}$$

with null and alternative hypothesis:

$$\mathcal{H}_0(\text{white noise}) : \hat{\rho}(k) = 0 \quad \forall k \neq 0$$

$$\mathcal{H}_1(\text{coloured noise}) : \hat{\rho}(k) \neq 0 \quad \text{for some } k \neq 0.$$

Under the null hypothesis, the statistic

$$Q_m = N(N+2) \sum_{k=1}^{m} \frac{\hat{\rho}^2(k)}{N-k}$$

asymptotically follows a Chi-squared distribution with m degrees of freedom (χ_m^2). Fig. 1 shows the obtained Q_m values for $m = 1, 2, \ldots, 100$ together with the threshold values at which, we would reject the null hypothesis at $\alpha_{sig} = 0.05$ significance level[4]. The obtained values are far above the thresholds which means that the null hypothesis can be rejected with a very low error probability (p). Actually, the p values obtained from our data are all below $2.22 \cdot 10^{-16}$ (simulation floating point accuracy),

[3]The setup conditions for the LOS experiment are given in Section IV (see Figure 3). The absence of shadowing obstacles and nearby objects prevented for correlation effects due to temporal fading.

[4]The null hypothesis would be rejected with 5% error probability.

TABLE I
TABLE OF KEY SYMBOLS

Symbol	Description
P_x, P_y	Transmitting, receiving power
d, d_0	Distance between transmitter and receiver and reference distance
$PL, \overline{PL}$	Propagation loss and average propagation loss
$X, \overline{X}$	Perturbation of signal strength, average value
S_w, S_X	PSD, its two-side version
σ	Standard derivation of the perturbation
f	Frequency
N_0	Noise power density
N	Number of measurements
$\hat{\rho}, Q_m$	Statistic to test the sample autocorrelation coefficient
p	Null hypothesis error probability
τ	correlation interval
t_m, M	Time stamps, total number of stamps
σ_τ^2	AVAR
T_s	Sampling time
χ_m^2	Chi-squared distribution with m degrees of freedom
α	Order of noise components
$A - E$	Coefficients of noise terms in time domain
h_α	Coefficients of noise terms in frequency domain
f_h, w_h	Bandwidth of the measurement system, angular expression
$H(z)$	z transform for generalized Wiener model
Q_d	Variance of input noise process
a_k, b_k	Coefficients of the MA, and AR models
z	Observed signal
w_α	Observation noise terms
i	Deterministic control input term
$\mathbf{s}$	State vector
$\mathbf{u}$	Driving noise vector
$\mathbf{A}$	State transition matrix for EKF models
$\mathbf{B}$	Driving noise transformation matrix
$h(\cdot), \mathbf{H(t)}$	Nonlinear transformation of the observation, its Jacobian
$a(\cdot), \mathbf{A(t)}$	Nonlinear transformation of the state vector, its Jacobian
$\mathbf{Q}$	State noise covariance matrix
$\mathbf{P}$	Estimation error covariance matrix
$\mathbf{K}$	Kalman gain
$\mathbf{I}$	Identity matrix

meaning that the probability of incorrectly assuming that the noise is not white would be lower than that.

The results of this test show that the noise present in the RSS measurements has a time-dependency statistical behaviour. In order to analyze this noise, the instrument of AVAR will be introduced as an effective tool to identify the noise components. We will show that AVAR constitutes a flexible tool to characterise any type of correlated noise term.

B. Allan Variance

The Allan variance (AVAR) was proposed by David W. Allan to characterise the underlying noise processes of clock systems in 1966 [24] and, together with some modifications, it has been recommended as a standard for such purpose [35]. Let $X(t)$ be the noise signal under study. The AVAR is obtained for different
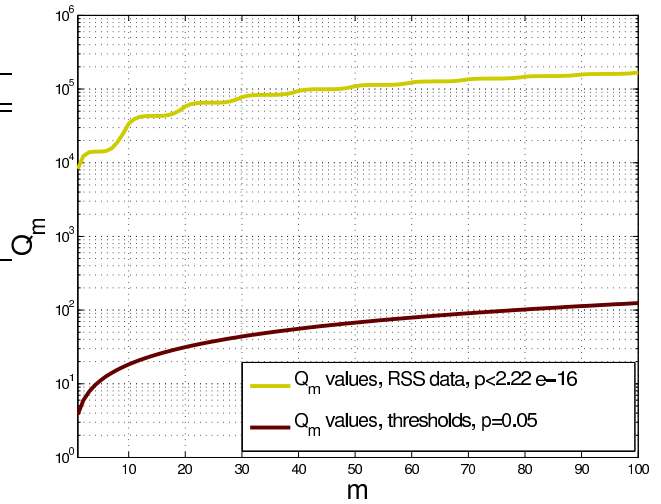

Fig. 1. Ljung-Box Q-test statistics obtained for $m = 1, 2, \ldots, 100$ time lags from $N = 15000$ RSS samples. Threshold values for $\alpha_{sig} = 0.05$ are also presented.

time stamps t_m as:

$$\sigma_\tau^2 = \frac{1}{2}\text{Var}\{\overline{X}(t_m + \tau) - \overline{X}(t_m)\} = \frac{1}{2}\text{Var}\{\overline{X}_{m+1} - \overline{X}_m\} \quad (4)$$

where

$$\overline{X}_m = \frac{1}{\tau}\int_{t_m}^{t_m+\tau} X(t)dt \quad (5)$$

and, for stationary processes, is only a function of τ. The sampling period is 100ms in our experiments. With this in mind, the AVAR can be easily estimated by numerically computing (5) as a sample average for different time instants t_m, $m = 1, ..., M - 1$ and the AVAR as a sample variance (note that $\text{E}\{\overline{X}_{m+1} - \overline{X}_m\} = 0$ for stationary processes):

$$\hat{\sigma}_\tau^2 = \frac{1}{2(M-1)}\sum_{m=1}^{M-1}(\mu_{m+1} - \mu_m)^2 \quad (6)$$

where

$$\mu_m = \frac{1}{K}\sum_{k=1}^{K} X(t_m + kTs)$$

with T_s the sampling time and $K = \lfloor \tau/T_s \rfloor$. The number of available samples M to calculate the sample variance is a function of the total length of the signal $N \cdot T_s$ and the integration interval τ:

$$M = \lfloor \frac{NT_s}{\tau} \rfloor$$

It is worth noting here that the error of the AVAR estimator, usually decreases as the averaging time τ increases. Confidence intervals for the estimation can be established by considering the distribution of the sample variance. Thus, we can use the Chi-squared distribution to establish its confidence interval as follows

$$\chi^2 = \frac{F\hat{\sigma}_\tau^2}{\sigma_\tau^2},$$

where σ_τ^2 is the true variance value and F is the number of degrees of freedom (DOF) of the estimator[5]. χ^2 denotes the cumulative distribution function (CDF) of the chi-squared distribution. Given a confidence of ε, the confidence interval for the Allan variance

[5]The number of DOF should be specifically estimated since the samples used for computing AVAR are seldom uncorrelated.

estimation is given by

$$\frac{F\hat{\sigma}_\tau^2}{\chi^2(\varepsilon)} \leq \sigma_\tau^2 \leq \frac{F\hat{\sigma}_\tau^2}{\chi^2(1-\varepsilon)}.$$

Because the error term $X_\sigma(t)$ in (3) may be composed of multiple components, it is important to count on a flexible representation of the power-law PSD so that the contribution of each component can be taken into account. Therefore, we apply the AVAR tool in this paper in order to not only obtain their contributions but also to apply them in practice. Power-law processes have been proved to be accurate instruments for representing the intrinsic properties of coloured noise an its PSD [36]–[38]. Let us consider a (one-sided) PSD which can be reasonably used to model the random fluctuations in RSS signals:

$$S_X(f) = \sum_\alpha h_\alpha f^\alpha, \qquad (7)$$

In practice, these random fluctuations can often be represented by the sum of five stochastic processes $-2 \leq \alpha \leq 2$ assumed to be independent [24], [35].

As described in [24], coloured noise is a combination of several types of components which cover different frequency bands of the noise spectrum. Similar to [24] and the IEEE standard [35], we only consider the major components which contribute the most part of the noise spectrum and AVAR values. Specifically the following 5 components: $-2 \leq \alpha \leq 2$ are analyzed. Some details of these noise components are introduced below [36]:

- Brow(nian) noise ($\alpha = -2$): This type of noise corresponds to a random walk behavior of the received signal [11]. Its origin is actually Brownian motion in the receiver circuitry.
- Pink noise ($\alpha = -1$): This component, also referred to as flicker noise, shows a $1/f$ pattern. It has a variety of different causes, usually related to the flow of direct current.
- White noise ($\alpha = 0$): Named by analogy to white light, with a flat frequency spectrum. As a wideband noise, RSS measurements have the equivalent component of white noise denoted by (3). The source of this noise can be thermal noise from the antennas and transceiver circuit or random shadowing effects [10] of the propagation channel.
- Blue noise ($\alpha = 1$): With a f increasing law, this term is sometimes loosely used to describe noise with minimal low frequency components. The specific origin is not well known, but one possible source is from the interference mitigation circuit which helps combat interference and improve the wireless signal quality [39].
- Violet noise ($\alpha = 2$): This noise presents a f^2 law and is also referred to as purple noise or differentiated white noise. Our results are aligned with no previously reported evidence of its presence in RSS measurements (to the best of our knowledge).

Specifically, for the model in (7), and considering the bounds for α, the AVAR can be expressed in the time domain as [36]:

$$\sigma_\tau^2 \approx Ah_{-2}\tau + Bh_{-1} + \frac{Ch_0}{\tau} + \frac{Dh_1 + Eh_2}{\tau^2} \qquad (8)$$

with the mapping coefficients given by

$$A = \frac{2\pi^2}{3}, \ B = 2\ln(2), \ C = \frac{1}{2},$$
$$D = \frac{1.038 + 3\ln(w_h\tau)}{4\pi^2}, \ E = \frac{3f_h}{4\pi^2},$$

where $f_h = w_h/(2\pi)$ is the bandwidth of the measurement system.

The h_α coefficients can be estimated using Least Squares (LS)

algorithms [40]. We showed in [41] that the introduction of AVAR to characterise the noise PSD is preferable to (for instance) directly fitting (7) using the periodogram. To illustrate this, we conducted a simple experiment (see the applications in Section V-A for the detailed procedure): We generated 1000 realizations (where each one has $N = 2^{14} = 16384$ samples) of a noise process whose PSD is given by (7) with $h_{-2} = 0.01, h_{-1} = 1, h_0 = 100, h_1 = 0, h_2 = 0$ as in [40]. For each of them, we estimated the two sets of h_α values using LS to fit the AVAR curve ($\hat{h}_\alpha^\sigma$) and the PSD directly estimated with the periodogram ($\hat{h}_\alpha^{PSD}$), respectively, for the sake of comparison. The histograms for the relative errors $e_\alpha^i = (\hat{h}_\alpha^i - h_\alpha)/h_\alpha$ are presented in Fig. 2, where lower values and dispersion can be observed for the AVAR case.

As we will show in the experimental section, the power-law identities present in RSS noise components can lead to simpler analyses if they are handled correctly. We will use the Least Squares (LS) algorithm to characterise the noise components through a parametric estimation of the AVAR as a power series (8). As shown in [41] and studied in Section III-B (see Fig. 2), the estimation method based on AVAR is preferable to direct estimation in the frequency domain based on the PSD. The noise characterisation is performed by taking advantage of the one-to-one relationship between the parametrization of AVAR and the noise PSD [see (8)].

We treat RSS coloured noise components as power-law processes so that they can be identified and analyzed even without the details of each noise source. Usually it is not a trivial task to identify the exact origin of each noise component. For example, [39] found that the wireless signal processing module of some peripheral cards can generate coloured noise. Specifically these network chipsets automatically increase the operational signal level and carrier sense threshold in order to ensure a certain level of signal to interference and noise ratio and the successful demodulation of incoming signals. Thus their RSS measurements usually follow a random walk behaviour, but statistically drift towards higher values with the increase of running time. The AVAR tool employed in this paper is able to analyze such time dependent behaviour even if such mechanism of the inner circuit is unknown. Furthermore, the flexibility of the power law PSD representation in eq. (8), allows for proper characterisation of correlated perturbations due to actual temporal fading (reflections, shadowing, etc), with no need to identify the dominating propagation mechanisms. This means that the α noise components can be used to model these perturbations even when their origin is not due to the specific types of noise mentioned above.

IV. EXPERIMENTS

This section characterises the correlated components of RSS perturbations using AVAR and the LS algorithm for model fitting. We carried out three groups of experiments, where different datasets were collected. The three scenarios under consideration are: different setups of the propagation environment, modifications of both transmitter and receiver hardware, and change of time span for parameter estimation. For the sake of comparison, we have simulated reference datasets perturbed with white noise whose mean and standard deviation are directly calculated from the obtained data. For each experiment, we show the result of the two datasets simultaneously in order to highlight the different characterisations of coloured and correlated perturbations and white noise. We also introduce the fitting curve given by LS algorithm to obtain the corresponding coefficients h_α of the RSS datasets.
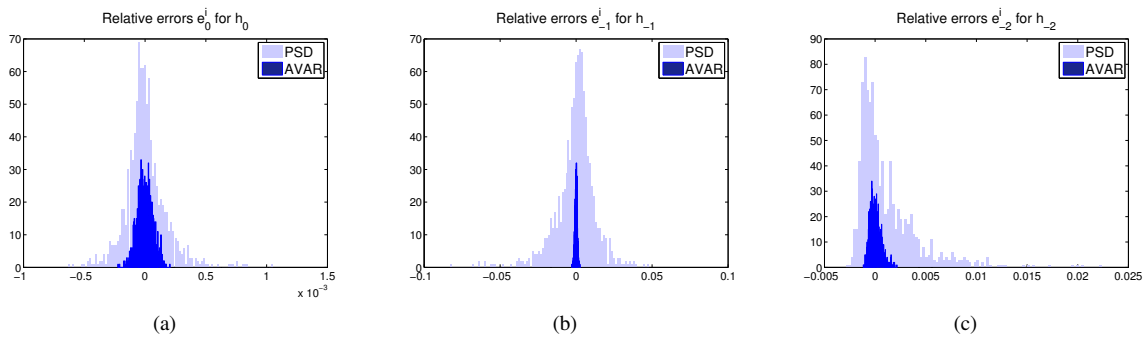
Fig. 2. Distribution of the relative estimation errors for h_0 (a), h_{-1} (b) and h_{-2} (c) coefficients using AVAR. The results obtained from direct estimation using the periodogram are also presented and denoted as PSD in the above figures.

A. Modification of the Propagation Environment

Three experiments were carried out to investigate the AVAR parameters regarding different fading/noise environments: 1) LOS signals with neither shadowing nor reflections; 2) The environment included both LOS and reflected signals from two plastic mattresses; 3) Shadowing environment with a human being completely blocking the LOS signals.

We set the experiment platform in the centre of a basketball court (size: 28m*15m) which did not have active RF equipment around. It was composed of an ASUS RT-N66U transmitter and a Lenovo T60 receiver, sitting on two plastic seats respectively, as shown in Fig.3. The carrier frequency (central frequency) was set to 5.22GHz (WLAN Channel 44). A frequency scanner was used to check that the RF environment was free from interference. The transmitter constantly broadcast BEACON signals every 100ms, which were received and demodulated by the receiver. Each experiment lasted approximately 1 hour. We then used an off-line application to extract the RSS measurements with time stamps from the original received packets. The mean removed RSS measurements were analysed to identify their components, which were presented in the figures.

The model coefficients h_α of these data are calculated using the LS algorithm and listed in Table II. Fig.4-6 show the AVAR values of the datasets with correlated components and those of the reference artificial white noise respectively, together with the LS fitted curve.

Analysis of the results

From Fig.4 - Fig.6 and Table II, we can see that because of the existence of correlated components, the AVAR curves of the RSS measurements do not decrease linearly with the increase of correlation time τ on the log-log diagram, whereas those with artificial white noise do follow this linear law. We can thus conclude that the traditional white noise assumption is inaccurate in every case (X_σ in (3)). This could be expected in all the cases except LOS, since fading due to either reflections or shadowing is present. However, for the LOS case, our experiment shows that the noise does also have coloured components, as opposed to the majority of approaches which generally assume white noise in these situations.

More specifically, the experiments show that the scenarios with LOS signals are closer to the assumption of white noise. Such trend diminishes with the degradation of the propagation environment following reflection and human being blocks. In detail, Fig.4 presents the white noise component (h_0) as the dominant one which is coloured by a Brownian noise term h_{-2}. Fig.5 presents both white noise (h_0) and $1/f$ terms (h_{-1}), the latter respectively accounting for reflections and shadowing. Fig.6 shows that the
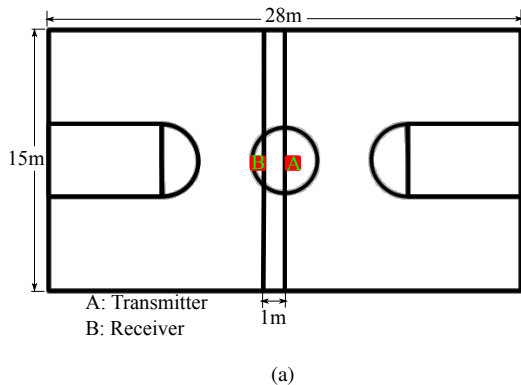

(a)

(b)

Fig. 3. Exemplar settings of the experiment environment and platform.

strong shadowing imposes a dominant $1/f$ component (h_{-1}), with meaningful contribution from the Brownian (h_{-2}) component. These two terms make the contribution of the white noise term negligible. Overall, the AVAR calculations do not show clear contributions from the f and f^2 components (h_1 and h_2).

B. Change of the Time Span

The following experiment aims to answer the question whether the characterisation obtained using AVAR coefficients changes over time or not. The same datasets from IV-A can be used since each of them was acquired in consecutive time slots. If meaningful changes over time do exist, distinctive coefficients would be obtained based on different periods of data. Therefore, we divided each dataset into two equal halves where the first half was acquired earlier than the second one. These sub-datasets were then analysed to obtain the AVAR coefficients.

TABLE II
MODEL PARAMETERS h_α OBTAINED FROM DIFFERENT PROPAGATION ENVIRONMENTS.

AVAR h	LOS	LOS+Reflection	NLOS(Human)
h_{-2}	$1.49497 \cdot 10^{-05}$	$3.22435 \cdot 10^{-14}$	0.00651
h_{-1}	$3.03409 \cdot 10^{-10}$	0.003110	0.77365
h_0	0.09220	0.122037	$2.69637 \cdot 10^{-13}$
h_1	$2.22057 \cdot 10^{-14}$	$2.22065 \cdot 10^{-14}$	$2.22046 \cdot 10^{-14}$
h_2	$2.22070 \cdot 10^{-14}$	$2.22711 \cdot 10^{-14}$	$2.22046 \cdot 10^{-14}$

TABLE III
MODEL PARAMETERS h_α OF THE MEASUREMENTS OBTAINED IN TWO CONSECUTIVE TIME PERIODS. THE SYMBOLS 1st AND 2nd DENOTE THE FIRST AND SECOND HALF OF THE CORRESPONDING DATASET.

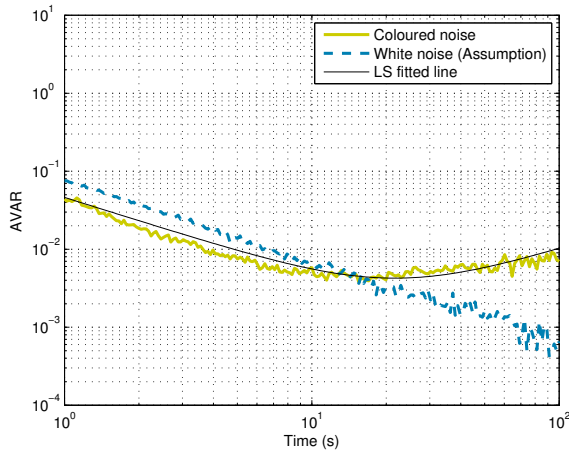| h	LOS		LOS+Reflection		NLOS(Human)	
	1st	2nd	1st	2nd	1st	2nd
h_{-2}	$1.10 \cdot 10^{-05}$	$2.01 \cdot 10^{-05}$	$2.89 \cdot 10^{-14}$	$2.93 \cdot 10^{-14}$	0.00641	0.00602
h_{-1}	$2.28 \cdot 10^{-09}$	$6.09 \cdot 10^{-09}$	0.00230	0.00367	0.74122	0.83067
h_0	0.10806	0.07656	0.13845	0.11163	$1.47 \cdot 10^{-07}$	$4.12 \cdot 10^{-08}$
h_1	$2.22 \cdot 10^{-14}$	$2.23 \cdot 10^{-14}$	$2.22 \cdot 10^{-14}$	$2.22 \cdot 10^{-14}$	$8.82 \cdot 10^{-14}$	$2.71 \cdot 10^{-14}$
h_2	$2.22 \cdot 10^{-14}$	$5.06 \cdot 10^{-14}$	$2.30 \cdot 10^{-14}$	$2.22 \cdot 10^{-14}$	$2.22 \cdot 10^{-14}$	$2.22 \cdot 10^{-14}$

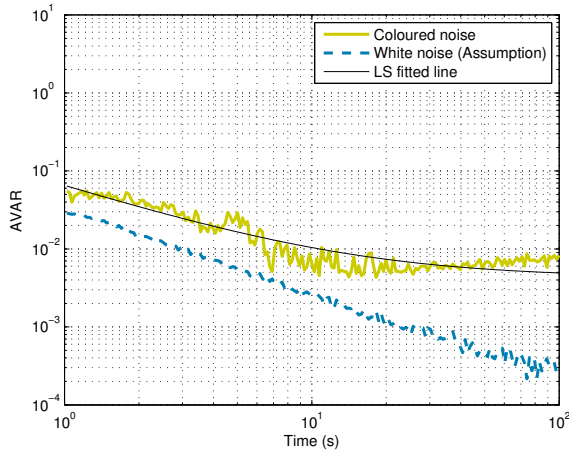Fig. 4. AVAR and the LS fitted line of the LOS scenario.

Fig. 5. AVAR and the LS fitted line of the NLOS scenario with plastic foam blocks.

Table III summarises the experiment results. In each dataset, the dominant component does not change over time, but the
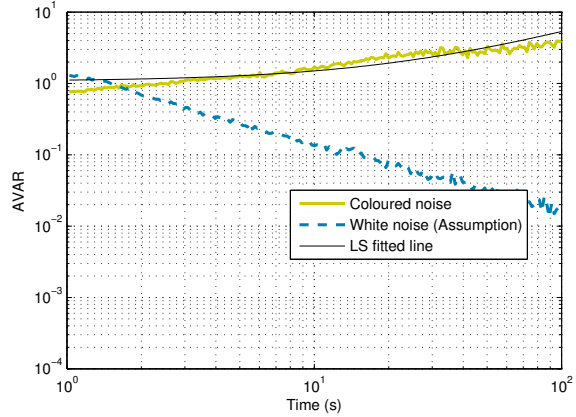

Fig. 6. AVAR and the LS fitted line of the NLOS scenario with a human block.

combination and contribution from each component may vary a little over time due to adjustment issues. In detail, the LOS dataset mainly has white noise (h_0); the reflection dataset has clear contributions from white noise (h_0) and $1/f$ perturbations (h_{-1}), which mainly accounts to the temporal fading; the dataset with human blocks is mainly affected by both flicker (h_{-1}) and Brownian (h_{-2}) components accounting for the shadowing. This experiment confirms that the proposed method does provide stable characterisation of RSS perturbations, and is useful for further processing in order to compensate or avoid the impact coming from coloured/correlated random terms.

C. Change of the Distance between Transmitter and Receiver

The next experiment investigates the influence of changing the distance between transmitter and receiver towards the components of the RSS perturbations (AVAR coefficients) in the LOS scenario. The other conditions remain unchanged. Table IV demonstrates the results, from which we can easily see that both the two cases have the same dominant noise (h_0), but the amounts have varied. In the case of "2m" distance, the $1/f$ component emerges as a small contribution whereas the remaining ones have greater weights. The origin of these correlated terms may be due to

AVAR h	1m	2m
h_{-2}	$1.49 \cdot 10^{-05}$	$4.90 \cdot 10^{-05}$
h_{-1}	$3.03 \cdot 10^{-10}$	0.000903
h_0	0.09220	0.070940
h_1	$2.22 \cdot 10^{-14}$	$9.99 \cdot 10^{-07}$
h_2	$2.22 \cdot 10^{-14}$	$9.99 \cdot 10^{-07}$

temporal fading caused by contributing reflections (e.g. floor) which are non-negligible in this new setup.

D. Different Hardware Setups

In order to examine the impacts of different hardware towards the corresponding AVAR parameters, we carried out two groups of experiments for the scenario of LOS signals using different hardware sets. Hardware-1 used an ASUS RT-N66U card for transmitter and an Intel PRO/Wireless 3945ABG card mounted on a Lenovo Thinkpad T60 laptop as the receiver, while hardware-2 used two Gigabyte GN-WI01GT cards for transmitter and receiver, respectively. The distances between transmitter and receiver are both set to 2m.

AVAR h	Hardware-1	Hardware-2
h_{-2}	$4.903 \cdot 10^{-05}$	$2.337 \cdot 10^{-14}$
h_{-1}	0.000903	0.020693
h_0	0.070940	0.984316
h_1	$9.999 \cdot 10^{-07}$	$1.060 \cdot 10^{-7}$
h_2	$9.999 \cdot 10^{-07}$	$7.545 \cdot 10^{-10}$

From Table V, we can see that different hardware settings can have large estimation discrepancies about the AVAR parameters, but they do not significantly change the relative weights of the different noise components, which are more related to the actual noise power. For example, the dominant noise in these two cases is still white (h_0), and the next component in terms of significance is flicker noise (h_{-1}), which lays on the interval $10\% - 20\%$ of the former. In order to deal with the inevitable hardware diversity, practical scenarios such as distance estimation can employ an estimation algorithm or a calibration procedure to improve the accuracy of a specific application.

E. Comparison with straightforward estimation using spectral methods

Commonly employed characterization procedures for coloured noise rely on the definition of parametric models for the PSD which consider specific contribution from each noise component. By adjusting the parametric equation in the frequency domain (e.g. using the periodogram), the different noise levels can be estimated. However, as we showed in [41], the use of the periodogram (specially when estimated through the Discrete Fourier Transform) is prone to errors when the PSD shows a significant frequency-dependant behaviour, especially for power-law densities [37]. Exploring alternative approaches is thus preferable.

Fig. 7 compares the obtained results in the first experiment with an estimation of the PSD of the noise obtained from the periodogram. The flicker ($\alpha = -1$) and white noise ($\alpha = 0$)

contributions can be easily appreciated in the figure while the random walk contribution ($\alpha = -2$) is not so obvious due to its low value. The significant frequency peak at $f = 1 Hz$ prevents from proper identification of the white noise contribution, which leads to a poor fitting of the PSD model if the periodogram estimation is directly employed. The theoretical fittings obtained from both the AVAR and PSD estimations are also shown in the figure. In fact, the values obtained from the latter tend to overestimate the white noise component and underestimate the other $1/f^\alpha$ coefficients. This can be observed in the figure where the negative slope of the PSD fitting is lower in absolute value, and the constant noise floor is reached at lower frequencies. On the other hand, the fitting obtained using AVAR better follows the PSD curve, featuring the same slope and reaching the noise floor level at the expected frequencies.
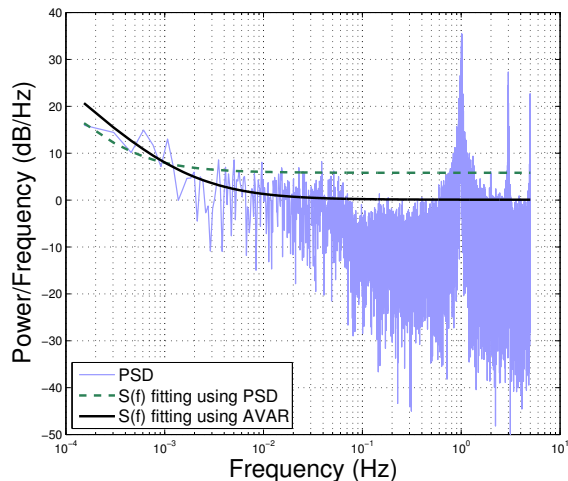

Fig. 7. PSD estimation of the RSS signal with theoretical fittings using both Allan and direct estimation via periodogram.

F. Experiments on a different dataset

The next group of datasets were collected by Caleb Phillips and Eric W. Anderson from the University of Colorado [42]. Different from the previous indoor experiments, the data were collected in an open flat flood plain where the distance between transmitter and receiver is about 100 feet. The researchers recorded RSS measurements received at each 5 degree azimuth position. In order to control the length of this article, we picked the two typical azimuth angles 0, 90 degrees, and processed the datasets at these directions.

Each of these datasets contains 80s of measurements. Comparing with the datasets collected in the previous experiment, the length is shorter. The AVAR calculations only cover a short correlation time interval, e.g. up to 80s. Nevertheless, the effects of coloured noise can still be observed from the results. Fig.8 - Fig.9 show the RSS measurements and the corresponding AVAR values, together with the comparable datasets with artificial white noise. The coefficients of the five types of noise components are listed in Table VI.

The results demonstrate fairly stable combination of noise, where the major contributions come from Brownian, Pink and White Noise for the first dataset, and Brownian and White Noise for the second dataset. The difference in this case is from the antenna effects where data received from the side lobe of the antenna may affect the contributions of different noise.
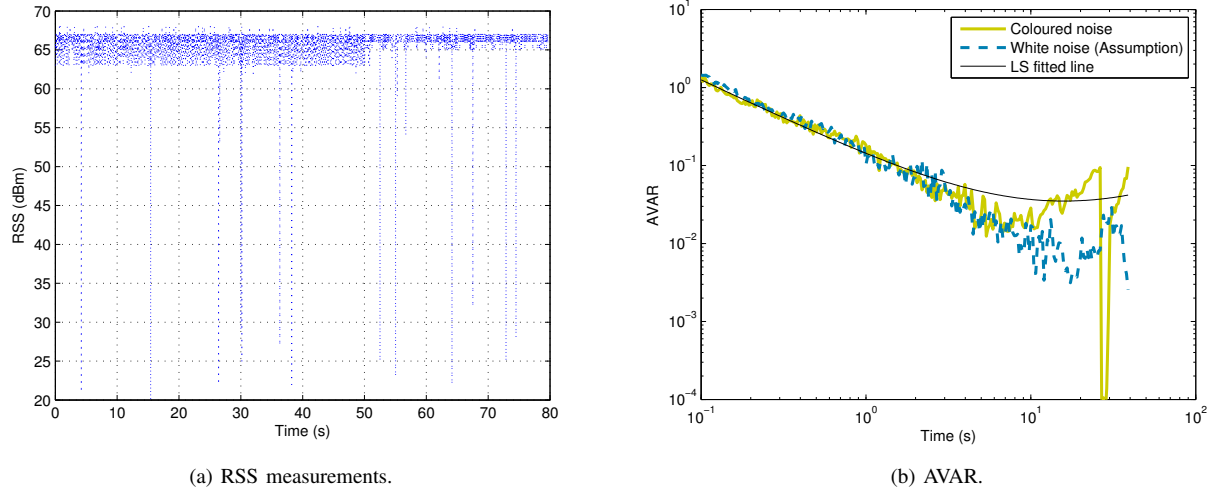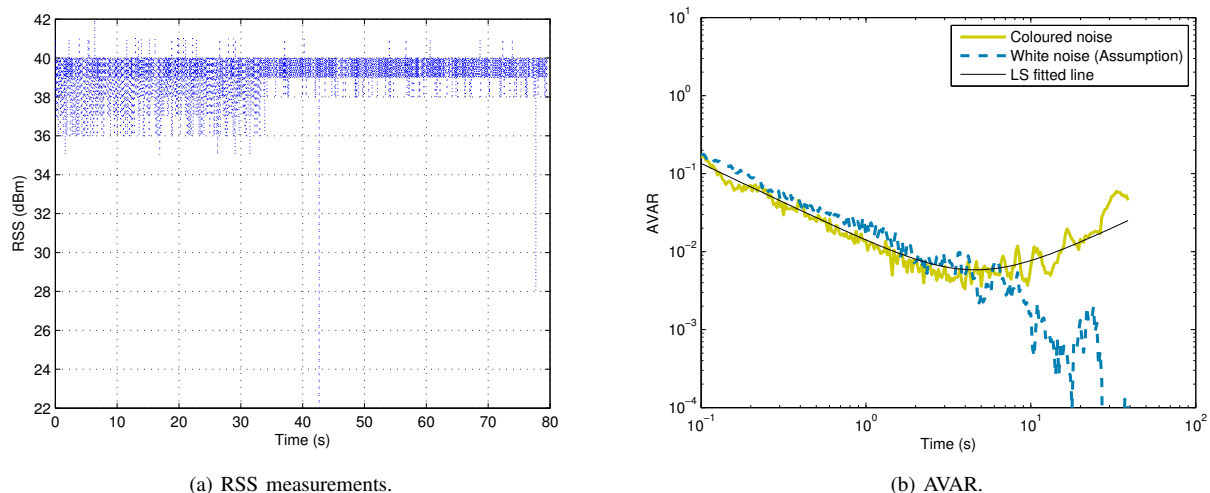
(a) RSS measurements.

(b) AVAR.

Fig. 8.   The RSS measurements and AVAR (0 degree).

(a) RSS measurements.

(b) AVAR.

Fig. 9.   The RSS measurements and AVAR (90 degree).

TABLE VI
PARAMETER h_α OF THE FLOOD PLAIN DATASET.

AVAR h	$0°$	$90°$
h_{-2}	0.000075	0.000096
h_{-1}	0.014009	8.138e-8
h_0	0.017734	0.026985
h_1	1.046e-12	9.999e-7
h_2	2.402e-14	9.997e-7

V. NOISE MODELLING AND PROCESSING

The experiments for AVAR and RSS measurements show distinctive differences from the assumption of only white noise, suggesting the existence of other noise components even when little fading exists. While the traditional assumption of white noise provides a feasible framework in modelling RSS, the discovery in our experiments sheds light on more accurate signal modelling and noise processing. This is particularly important for applications involving time varying processes, e.g. tracking positions of vehicles or mobile robotic equipment.

The advantage of AVAR for characterising perturbations for noise type identification through log-log representation paves the road for noise synthesis and real-world applications such as position estimation. In particular, practical measurements of RSS signals show favourably stable combination of noise types, which can be characterised by AVAR and used to determine parameters of system models. In this section we illustrate two applications of the present study:

1) Noise synthesis for simulation purposes. We introduce a simple method based on Wiener processes which allows incorporation of coloured noise components into the generation of artificial datasets.

2) Position estimation using RSS. We propose a method based on the extended Kalman filter which considers the coloured noise components. According to [43], Extended Kalman filter is a standard method for tracking and navigation where the underlying transition incorporates non-linearity.

A. Simulation of RSS Noise

We are interested in simulating discrete noise processes following the PSD in (7) or, equivalently, its power-conserving two

sided version:

$$S_X(f) = \sum_\alpha \frac{h_{-\alpha}}{2} \frac{1}{|f|^\alpha} \tag{9}$$

Assuming statistically independent sources of these noise components [33], we can simulate them individually using the method from [37] and then adding the corresponding components to generate the final result. The simulation method consists in filtering a white noise process using the following generalized Wiener model

$$H(z) = \frac{1}{(1 - z^{-1})^{\alpha/2}}. \tag{10}$$

The spectral density of the filtered noise can be calculated through $S_d = \Delta t Q_d H(z) H(z^{-1})$ with $z = e^{j\omega\Delta t}$, Δt the sample time and Q_d the variance of the input noise process [44]:

$$S_d(f) = \frac{Q_d \Delta t}{(2 \sin(\pi|f|\Delta t))^\alpha}. \tag{11}$$

$S_d(f)$ can be approximated for the frequencies below the Nyquist limit as

$$S_d(f) \approx \frac{Q_d \Delta t^{1-\alpha}}{(2\pi|f|)^\alpha}, \tag{12}$$

which shows a power law property like the terms in (9). The input noise variance is thus selected by properly mapping (12) to each component of (9) so that it can be synthesized using the filter in (10):

$$Q_d = \frac{h_{-\alpha}}{2} \frac{(2\pi\Delta t)^\alpha}{\Delta t}. \tag{13}$$

The even α values yield filters which can be accurately implemented, such as the random walk model ($\alpha = 2$, see an example of the model description in Section V-B, equation (20)). For the odd values, an approximation needs to be made. In this case, the transfer function in (10) can be expanded as a pure moving average (MA) process:

$$H(z) = 1 + \frac{\alpha}{2} z^{-1} + \frac{\alpha/2(\alpha/2 + 1)}{2!} z^{-2} + ... \tag{14}$$

The coefficients of the z^{-k} terms in the above equation are given by

$$b_k = \prod_{n=1}^{k} (\alpha/2 + n - 1)/n. \tag{15}$$

An autoregressive (AR) process can be used as an alternative. In this case, the transfer function is expressed as [37]:

$$H(z) = \frac{1}{1 - \frac{\alpha}{2} z^{-1} - \frac{\alpha/2(1-\alpha/2)}{2!} z^{-2} + ...} \tag{16}$$

with the coefficients

$$a_k = \prod_{n=1}^{k} (n - 1 - \alpha/2)/n. \tag{17}$$

This approach is used in Section V-B to model flicker noise ($\alpha = 1$).

The simulation of coloured noise presents a number of applications which are extensible to other signal domains. For example, a straightforward one is the generation of synthetic signals to test theoretical hypotheses and algorithms as demonstrated in this paper. The procedure described here was used in Section III-B to show the appropriateness of using AVAR to characterise the noise PSD. The simulated noise in the time domain together with the corresponding PSD are shown in Fig.10. Another useful application can be the simulation of experimental frameworks which are not easy to set up in practice, e.g. a scenario with long distances between nodes and/or a controlled interference
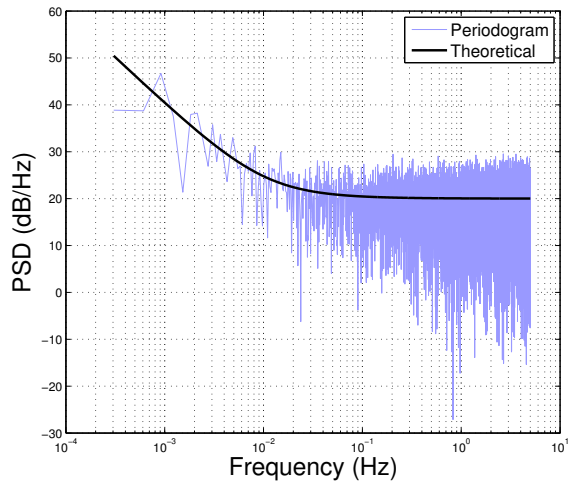
environment.

Fig. 10. PSD of the simulated RSS noise with $S(f) = 100 + \frac{1}{f} + \frac{0.01}{f^2}$.

B. Coloured Noise and RSS Localization

One of the most useful RSS applications is tracking and localisation, such as vehicle/robot tracking and wireless sensor networks. Since both correlated perturbations (including coloured noise) and white noise components are present in RSS acquisitions, the traditional models which only consider white noise should be modified to handle these correlated RSS components. This subsection considers localization algorithms with the extended Kalman filter as an example to demonstrate the method to deal with coloured noise. Based on the parameters estimated by AVAR, we integrate the path loss model in (3) with the Kalman filter so that the RSS signals can be used to track the distance between a transmitter and a receiver. The measurement equation can thus be reorganised as follows,

$$P_y(t) = P_y(d(0)) - 10n \log \frac{d(t)}{d(0)} + \sum_\alpha w_\alpha(t) \tag{18}$$

where we have expressed the perturbation $X_\sigma(t)$ in (3) as a sum of the correlated (coloured) ($\alpha \neq 0$) and white ($\alpha = 0$) components. Following our results in the experiments section, the random walk and flicker noise ($\alpha = -2, -1$ respectively) of the coloured components are considered. The state evolution for the distance can be written as:

$$d(t) = d(t - 1) + i(t - 1) + u_d(t) \tag{19}$$

where $i(t - 1)$ is an optional deterministic control input and $u_d(t) \sim \mathcal{N}(0, \sigma_d^2)$ represents the white evolution noise. Since we are dealing with coloured noise components, they need to be considered in the state equations. The Brownian noise can be modelled using a random walk process [45]:

$$w_{-2}(t) = w_{-2}(t - 1) + u_{-2}(t) \tag{20}$$

where $u_{-2}(t) \sim \mathcal{N}(0, \sigma_{-2}^2)$ is a realization of a white noise process with $\sigma_{-2}^2 = h_{-2}(2\pi\Delta t)^2/(2\Delta t)$ [see (13)]. The unlimited bandwidth of $1/f$ noise imposes an approximation for the flicker component. Following the last procedure described in Section V-A, we can use a p-order autoregressive (AR) model:

$$w_{-1}(t) = -\sum_{k=1}^{p} a_k w_{-1}(t-k) + u_{-1}(t) \qquad (21)$$

with $u_{-1}(t) \sim \mathcal{N}(0, \sigma_{-1}^2)$ a white noise process with $\sigma_{-1}^2 = h_{-1}\pi$ according to (13) and the a_k coefficients given by (17) with $\alpha = 1$. The state vector is thus defined using a Gauss-Markow process [46]: $\mathbf{s}(t) = [d(t), w_{-1}(t), w_{-1}(t-1), \ldots w_{-1}(t-p+1), w_{-2}(t)]^T$. Without loss of generality, we can remove the deterministic control input from the equation and set the state evolution as

$$\mathbf{s}(t) = \mathbf{A}\mathbf{s}(t-1) + \mathbf{B}\mathbf{u}(t) \qquad (22)$$

with $\mathbf{u}(t) = [u_d(t), u_{-1}(t), u_{-2}(t)]^T$. The state transition matrix is

$$\mathbf{A}_{(p+2)\times(p+2)} = \begin{bmatrix} 1 & 0 & 0 & \ldots & 0 & 0 \\ 0 & -a_1 & -a_2 & \ldots & -a_p & 0 \\ 0 & 1 & 0 & \ldots & 0 & 0 \\ 0 & 0 & 1 & \ldots & 0 & 0 \\ \vdots & \vdots & \vdots & \vdots & \vdots & \vdots \\ 0 & 0 & 0 & \ldots & 0 & 1 \end{bmatrix}, \qquad (23)$$

and the driving noise vector is transformed by

$$\mathbf{B}_{(p+2)\times 3} = \begin{bmatrix} 1 & 0 & 0 \\ 0 & 1 & 0 \\ \vdots & \vdots & \vdots \\ 0 & 0 & 0 \\ 0 & 0 & 0 \\ 0 & 0 & 1 \end{bmatrix}. \qquad (24)$$

The implementation of the extended Kalman filter is based on the observation (18) and state (22) equations. We rewrite the observation equation as

$$z(t) = h(\mathbf{s}(t)) + w_0(t), \qquad (25)$$

where $w_0(t) \sim \mathcal{N}(0, \sigma_0^2)$ is the RSS measurement white noise component whose variance is obtained as $\sigma_0^2 = h_0/(2\Delta t)$ according to (13). We calculate the Jacobian of $h(\cdot)$ as $\mathbf{H}(t)_{(p+2)\times 1} = [-10n/(\ln(10)d(t)), 1\ldots, 0, 0, 1]^T$.

The prediction equations can be obtained as follows

$$\hat{\mathbf{s}}^-(t) = \mathbf{A}\hat{\mathbf{s}}(t-1)$$
$$\mathbf{P}^-(t) = \mathbf{A}\mathbf{P}(t-1)\mathbf{A}^T + \mathbf{B}\mathbf{Q}\mathbf{B}^T \qquad (26)$$

where $\mathbf{Q}$ is the state noise variance matrix given by $\mathrm{diag}\{\sigma_d^2, \sigma_{-1}^2, \sigma_{-2}^2\}$ and $\mathbf{P}^-(t)$, $\mathbf{P}(t)$ are the updated and predicted estimation error covariance matrices respectively. The Kalman gain is given by

$$\mathbf{K}(t) = \mathbf{P}^-(t)\mathbf{H}(t)/(\mathbf{H}(t)^T\mathbf{P}^-(t)\mathbf{H}(t) + \sigma_0^2), \qquad (27)$$

the new state is

$$\hat{\mathbf{s}}(t) = \hat{\mathbf{s}}^-(t) + \mathbf{K}(t)(z(t) - h(\hat{\mathbf{s}}^-(t))), \qquad (28)$$

and the predicted error covariance is given by

$$\mathbf{P}(t) = (\mathbf{I} - \mathbf{K}(t)\mathbf{H}(t)^T)\mathbf{P}^-(t). \qquad (29)$$

In order to provide the model with more flexibility (e.g., cases in which the environment changes and thus the noise parameters can vary with time), the AR coefficients in (31) can be considered as time-varying to augment the state vector equations of the EKF. Equation (31) would turn into

$$w_{-1}(t) = -\sum_{k=1}^{p} a_k(t) w_{-1}(t-k) + u_{-1}(t) \qquad (30)$$

and the state vector would now be: $\mathbf{s}(t) = [d(t), w_{-1}(t), w_{-1}(t-1), \ldots w_{-1}(t-p+1), w_{-2}(t), a_1(t), \ldots, a_p(t)]^T$. The evolution of the AR coefficients can be modelled as independent random-walk processes:

$$a_k(t) = a_k(t-1) + u_{ak}(t). \qquad (31)$$

This would lead to a nonlinear state evolution equation:

$$\mathbf{s}(t) = \mathbf{a}[\mathbf{s}(t-1)] + \mathbf{B}\mathbf{u}(t) \qquad (32)$$

with $\mathbf{u}(t) = [u_d(t), u_{-1}(t), u_{-2}(t), u_{a1}(t), \ldots, u_{ap}(t)]^T$. The Jacobian of of $\mathbf{a}(\cdot)$ is: $\mathbf{A}(t)_{(2p+2)\times(2p+2)}$, given by

$$\begin{bmatrix} 1 & 0 & \ldots & 0 & 0 & 0 & \ldots & 0 \\ 0 & -a_1(t) & \ldots & -a_p(t) & 0 & -\psi(1) & \ldots & -\psi(p) \\ 0 & 1 & \ldots & 0 & 0 & 0 & \ldots & 0 \\ \vdots & \vdots & \vdots & \vdots & \vdots & \vdots & \vdots & \vdots \\ 0 & 0 & \ldots & 0 & 1 & 0 & \ldots & 0 \\ 0 & 0 & \ldots & 0 & 0 & 1 & \ldots & 0 \\ \vdots & \vdots & \vdots & \vdots & \vdots & \vdots & \vdots & \vdots \\ 0 & 0 & \ldots & 0 & 0 & 0 & \ldots & 1 \end{bmatrix},$$
$$(33)$$

where $-\psi(i) = -w_{-1}(t-i), i = 1, \ldots, p$ and the driving noise vector is now transformed by

$$\mathbf{B}_{(2p+2)\times(p+3)} = \begin{bmatrix} 1 & 0 & \ldots & 0 & 0 & 0 & \ldots & 0 \\ 0 & 1 & \ldots & 0 & 0 & 0 & \ldots & 0 \\ 0 & 0 & \ldots & 0 & 0 & 0 & \ldots & 0 \\ \vdots & \vdots & \vdots & \vdots & \vdots & \vdots & \vdots & \vdots \\ 0 & 0 & \ldots & 0 & 1 & 0 & \ldots & 0 \\ 0 & 0 & \ldots & 0 & 0 & 1 & \ldots & 0 \\ \vdots & \vdots & \vdots & \vdots & \vdots & \vdots & \vdots & \vdots \\ 0 & 0 & \ldots & 0 & 0 & 0 & \ldots & 1 \end{bmatrix}. \qquad (34)$$

The observation equation can also be written as (25). The Jacobian of $h(\cdot)$ is now $\mathbf{H}(t)_{(2p+2)\times 1} = [-10n/(\ln(10)d(t)), 1\ldots, 0, 0, 1, 0, \ldots, 0]^T$, and the prediction equations are

$$\hat{\mathbf{s}}^-(t) = \mathbf{a}[\hat{\mathbf{s}}(t-1)]$$
$$\mathbf{P}^-(t) = \mathbf{A}(t-1)\mathbf{P}(t-1)\mathbf{A}(t-1)^T + \mathbf{B}\mathbf{Q}\mathbf{B}^T \qquad (35)$$

where $\mathbf{Q}$ is extended to account for the time varying AR evolution noise, and the dimension of $\mathbf{P}$ is extended accordingly to $(2p+2) \times (2p+2)$. Equations (27)–(29) are not modified in this new EKF except for the different dimension of the involved terms.

We investigated the two proposed versions of the EKF with the static and dynamic coloured noise models running an experiment which was divided into two steps. The datasets were acquired firstly and processed to obtain the corresponding AVAR coefficients. These coefficients were then fed into the EKFs as described above. For the sake of comparison, we also implemented an EKF considering only white noise. The variance of the white noise was defined equal to the coloured noise one. The same parameter $\sigma_d = 0.003$ was used for the three EKFs. For performance assessment on varying distance estimation, we employed a flying Unmanned Aerial Vehicle (UAV) with a GPS receiver (Ublox LEA4T) to record position information, which was post-processed using reference information received by the GPS base station. With the usage of highly sensitive antennas and accurate
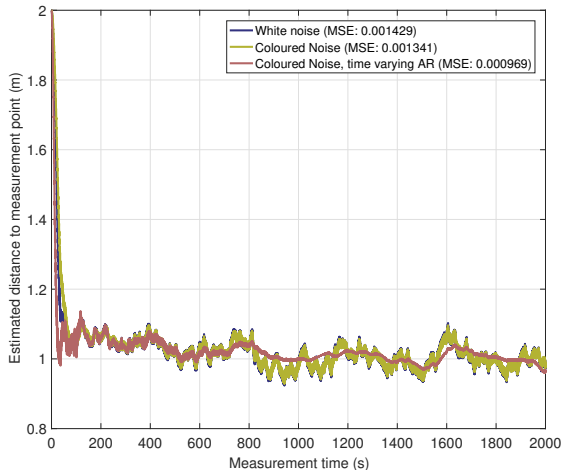
Fig. 11. Distance estimations obtained for the three compared EKFs. The figure insets present the MSE values with respect to the actual GPS-measured distance.
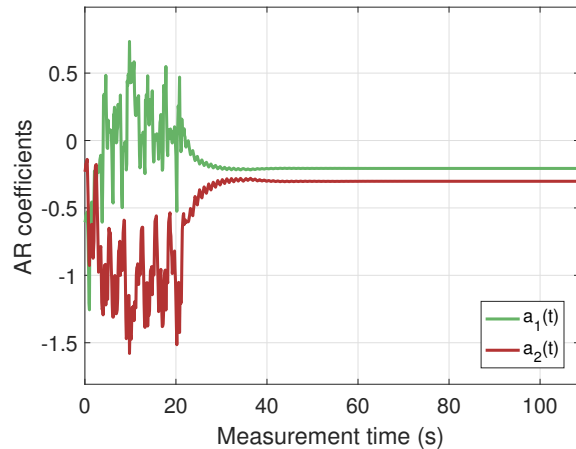

Fig. 12. Learning curves for time-varying AR coefficients included in the EKF model.

Fig. 13. UAV-to-transmitter stationary distance estimation vs. measurement time.

geographical information of the base station, the error between GPS measurements and UAV's true position is at the level of $10cm$, which is also confirmed by manual measurements. Three gyros (Analog Devices ADXRS610), a tri-axial accelerometer (Memsic MXR9500), three magnetometers (NXP KMZ51) and a pressure sensor (Freescale MPXH6115) are fused at the rate of 1KHz by the UAV's on-board firmware to provide the IMU data.

Fig.11 shows the obtained estimated distances from the measurement platform for the three EKF models. It can be easily appreciated that the static coloured noise model yields a less varying trajectory estimation at the expense of a slightly slower stabilization compared with the white noise EKF. On the other hand, the augmented EKF incorporating time-varying coloured noise parameter estimation, overcomes both static models, with both smaller acquisition time and variance in the estimation. This is highlighted in the figure inset, where the Mean Squared Errors (MSE) have been computed for the three filters, with the lowest values obtained for the time-varying parameter EKF. The learning curves for the time-varying AR coefficients are presented in Fig. 12, showing a quick stabilization which leads to the faster convergence of the time-varying model.

The next two experiments show the performance of the modelling strategy when applied for distance estimation in different scenarios including both stationary and mobile platforms.

The first one investigated the proposed EKF algorithm with the coloured noise model running an experiment where a receiver was used to locate a static object placed 1 m away. For the sake of comparison, we also implemented the EKF considering only white noise . Fig. 13 presents the results. We can easily see that the coloured noise model has higher accuracy than the white noise EKF algorithm during the majority of the measurement time.

Of particular interest in distance estimation is to evaluate the modelling strategy in a mobile environment. The second experiment used a flying UAV to record the RSS measurements of wireless signals and measured the ground-truth by means of a GPS receiver. Fig. 14 shows a scatter diagram of the distance estimation errors vs actual distance obtained from the EKF filter using our coloured noise model vs. a white noise model. It is easy to see that most distance errors for the coloured noise EKF model are less than 5m, while for the white noise model, the performance
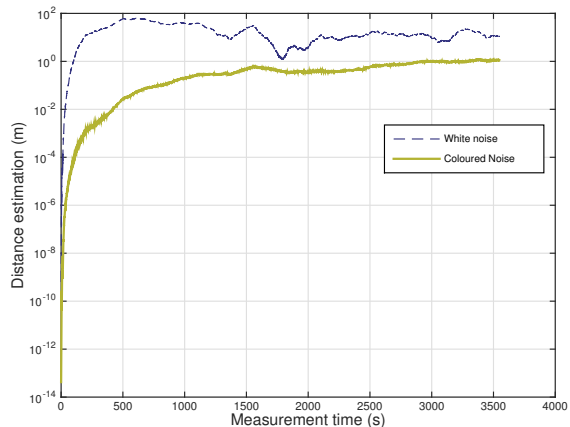
varies significantly and the majority of errors are greater than 5m. It is interesting to see that the errors of the coloured noise EKF model raise sharply at around 48-49m. This can be explained by a sudden signal loss during the movement of the UAV at greater distances, which can be compensated in real world applications by increasing the transmission power, or fusing multiple signals.

VI. DISCUSSION

This paper focuses on the analysis of random perturbations with distinctive AVAR or PSD. Results from our experiments show that the propagation environment has strong impact towards the combination of the random perturbation terms. Within the same environment, the change of measurement hardware or time does not affect the weight of the different PSD components. Therefore, they can be modelled by the coefficients h_α. Such treatment provides a tangible method in modelling and processing each perturbation component and their various combinations.

Inappropriate ways of measurement may add significant noise to the acquired RSS values. For WiFi signals, IEEE 802.11 [47], [48] or IEEE 802.15.4 [49], [50] standards are often implemented in the sensors or peripheral cards. In these devices, the signals are firstly demodulated and then converted to digital forms by the analog-to-digital converter, where useful signals are separated
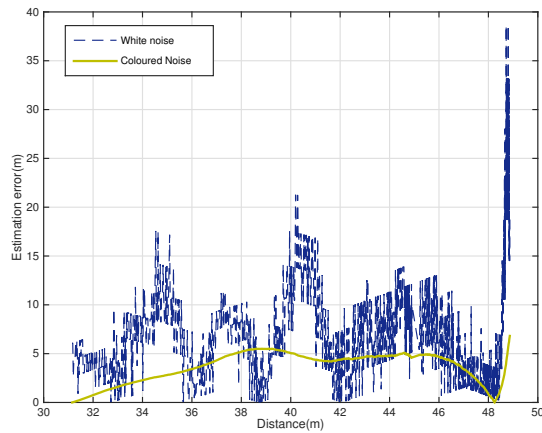
Fig. 14. UAV-to-transmitter mobile distance estimation error vs. actual distance.

from the circuit noise which usually appears to have a low noise floor, e.g. -95dBm. Packets and readings will be lost if the signal power is close to or below -95dBm. In order to avoid this problem, the receiving power should always be above such a noise floor. For example, in the previous experiments, the transmitting power was set to 20dBm to ensure a strong average receiving power level.

This paper analyses noise and other perturbations using 802.11 signals. However, the proposed methodology constitutes a general characterisation framework since it can be directly applied to various types of wireless signals following the propagation model. Besides, the noise synthesis application studied in Section V-A allows the simulation of coloured noise components that can be effectively used to design and test optimal reception algorithms for a number of signal models. As long as the noise of wireless signals follows the power-law property, similar instruments can be applied to identify and mitigate the corresponding coloured noise components. The findings of this paper present an improvement over traditional treatment of noise and the corresponding applications.

VII. CONCLUSION

This paper investigates the perturbation components of wireless signals in RSS modelling and measurements. We first introduced the radio frequency signal propagation model and analysed the textcolorblackperturbations in detail. Theoretically five components were defined, however, our experiments found only three major contributing components. The estimated coefficients from experiments, which denote the contributions of each component, can be modelled by a Wiener process as shown in Section V-A. We also briefly cover the issues of applying a Kalman filter under the presence of coloured noise. The method of analysis and results can be used in practical scenarios requiring accurate modelling and processing of RSS.

Our future research lines include the application of the EKF to track moving objects. Such scenarios are subject to continuous modifications of the propagation environment which may affect the values of the AVAR components. To account for these, we are currently working on the definition of evolution models for the h_α coefficients to incorporate into the EKF equations.

The EKF program and datasets are available on request.

REFERENCES

[1] A. Wadhwa, U. Madhow, J. P. Hespanha, and B. M. Sadler, "Following an RF trail to its source," in *Proc. of the 49th Annual Allerton Conf. on Comm., Contr., and Computing*, Sep. 2011.

[2] I. Guvenc, C. T. Abdallah, R. Jordan, and O, "Enhancements to RSS based indoor tracking systems using Kalman filters," *GSPx & International*, 2003.

[3] X. Li, "RSS-based location estimation with unknown pathloss model," *IEEE Trans. Wireless Commun.*, vol. 5, no. 12, pp. 3626 –3633, Dec. 2006.

[4] M. Mertens, M. Ulmke, and W. Koch, "Ground target tracking with RCS estimation based on signal strength measurements," *IEEE Trans. Aerosp. Electron. Syst.*, vol. 52, no. 1, pp. 205–220, Feb. 2016.

[5] A. Weiss, "On the accuracy of a cellular location system based on RSS measurements," *IEEE Trans. Veh. Technol.*, vol. 52, no. 6, pp. 1508 – 1518, Nov. 2003.

[6] T. Roos, P. Myllymaki, and H. Tirri, "A statistical modeling approach to location estimation," *IEEE Trans. Mobile Comput.*, vol. 1, no. 1, pp. 59 – 69, Jan. 2002.

[7] H. Friis, "A note on a simple transmission formula," in *Pro. IRE.* 34, 1946, pp. 254–256.

[8] A. Goldsmith, *Wireless communications*. Cambridge University Press, 2005.

[9] J. D. Parsons, *The Mobile Radio Propagation Channel*, 2nd ed. Wiley, Nov. 2000.

[10] T. S. Rappaporat, *Wireless Communications - Principle and Practice*. Prentice-Hall, 1996.

[11] J. G. Proakis, *Digital communications*, 4th ed. New York: McGraw-Hill, Inc., 2001.

[12] H. Hashemi, "The indoor radio propagation channel," *Proceedings of the IEEE*, vol. 81, pp. 943–968, 1993.

[13] A. Demir, "Phase noise in oscillators: DAEs and colored noise sources," in *1998 IEEE/ACM International Conference on Computer-Aided Design*, Nov. 1998, pp. 170–177.

[14] A. Demir, A. Mehrotra, and J. Roychowdhury, "Phase noise in oscillators: a unifying theory and numerical methods for characterization," *IEEE Trans. Circuits Syst. I, Fundam. Theory Appl. (1993-2003)*, vol. 47, no. 5, pp. 655–674, May 2000.

[15] A. Demir, "Phase noise and timing jitter in oscillators with colored-noise sources," *IEEE Trans. Circuits Syst. I, Fundam. Theory Appl. (1993-2003)*, vol. 49, no. 12, pp. 1782–1791, Dec. 2002.

[16] M. Gudmundson, "Correlation model for shadow fading in mobile radio systems," *Electronics Letters*, vol. 27, pp. 2145–2146, 1991.

[17] S. Wyne, A. Singh, F. Tufvesson, and A. Molisch, "A statistical model for indoor office wireless sensor channels," *Wireless Communications, IEEE Transactions on*, vol. 8, pp. 4154–4164, 2009.

[18] A. Aubry, V. Carotenuto, A. D. Maio, and A. Farina, "Radar phase noise modeling and effects-part ii: pulse doppler processors and sidelobe blankers," *IEEE Trans. Aerosp. Electron. Syst.*, vol. 52, no. 2, pp. 712–725, Apr. 2016.

[19] K. Pahlavan and A. Levesque, *Wireless Information Networks*, ser. Wiley Series in Telecommunications and Signal Processing. Wiley, 2005.

[20] R. Zekavat and R. Buehrer, *Handbook of Position Location: Theory, Practice and Advances*, ser. IEEE Series on Digital & Mobile Communication. John Wiley & Sons, 2011.

[21] P. Hänggi and P. Jung, "Colored noise in dynamical systems," *Advances in Chemical Physics*, vol. 89, pp. 239 – 326, 1995.

[22] Y. Stebler, S. Guerrier, J. Skaloud, and M. P. Victoria-Feser, "Generalized method of wavelet moments for inertial navigation filter design," *IEEE Trans. Aerosp. Electron. Syst.*, vol. 50, no. 3, pp. 2269–2283, Jul. 2014.

[23] Z. Malkin, "Application of the allan variance to time series analysis in astrometry and geodesy: A review," *IEEE Trans. Ultrason., Ferroelect., Freq. Control*, vol. 63, no. 4, pp. 582–589, Apr. 2016.

[24] D. Allan, "Statistics of atomic frequency standards," *Proceedings of the IEEE*, vol. 54, no. 2, pp. 221 – 230, Feb. 1966.

[25] X. Chen, D. Schonfeld, and A. Khokhar, "Localization and trajectory estimation of mobile objects using minimum samples," *IEEE Trans. Veh. Technol.*, vol. 58, no. 8, pp. 4439 –4446, Oct. 2009.

[26] C. Luo, S. McClean, G. Parr, L. Teacy, and R. Nardi, "UAV position estimation and collision avoidance using the extended Kalman filter," *IEEE Trans. Veh. Technol.*, vol. 62, no. 6, pp. 2749–2762, 2013.

[27] D. Arora and M. McGuire, "Lower bounds on mobile terminal localisation in an urban area," *IET Commun.*, vol. 5, no. 9, pp. 1182 –1191, June 2011.

[28] S. Cameron, S. Hailes, S. McClean, and et al., "Suaave: Combining aerial robots and wireless networking," in *SUAAVE*. University of Oxford, University College London, University of Ulster, Feb. 2010, pp. 1–14.

[29] D. C. Cox, R. R. Murray, and A. W. Norris, "800 MHz attenuation measured in and around suburban houses," *Bell Labs Tech. J.*, vol. 63, pp. 921–954, 1984.

[30] S. Seidel and T. Rappaport, "914 MHz path loss prediction models for indoor wireless communications in multifloored buildings," *IEEE Trans. Antennas Propag.*, vol. 40, no. 2, pp. 207–217, Feb. 1992.

[31] A. Einstein, *Investigations on the Theory of the Brownian Movement*, ser. Dover Books on Physics. Dover Publications, 1956.

[32] R. Short, L. Mandel, and R. Roy, "Correlation functions of a dye laser: Comparison between theory and experiment," *Phys. Rev. Lett.*, vol. 9, no. 49, pp. 647–650, Aug. 1982.

[33] L. C. Ng, "On the application of Allan variance method for ring laser gyro performance characterization," *Oct.*, p. 29, 1993.

[34] G. M. Ljung and G. E. P. Box, "On a measure of lack of fit in time series models," *Biometrika*, vol. 65, no. 2, pp. 297–303, 1978.

[35] "IEEE standard definitions of physical quantities for fundamental frequency and time metrology - random instabilities," *IEEE Std 1139-1999*, pp. 1–36, 1999.

[36] D. Allan, "Should the classical variance be used as a basic measure in standards metrology?" *IEEE Transactions on Instrumentation and Measurement*, vol. IM-36, pp. 646–654, 1987.

[37] N. J. Kasdin, "Discrete simulation of colored noise and stochastic processes and $1/f^{\alpha}$ power law noise generation," *IEEE Proc.*, vol. 83, no. 5, pp. 802–827, May 1995.

[38] J. Timmer and M. Knig, "On generating power law noise," *Astronomy and Astrophysics*, vol. 300, pp. 707–710, 1995.

[39] S. Robitzsch, L. Murphy, and J. Fitzpatrick, "An analysis of the received signal strength accuracy in 802.11a networks using atheros chipsets: A solution towards self configuration," in *IEEE GLOBECOM Workshops (GC Wkshps)*. IEEE, Dec. 2011, pp. 1429–1434.

[40] F. Vernotte, E. Lantz, J. Groslambert, and J. Gagnepain, "Oscillator noise analysis: multivariance measurement," *Instrumentation and Measurement, IEEE Transactions on*, vol. 42, no. 2, pp. 342–350, Apr 1993.

[41] C. Luo, P. C. de-la Higuera, S. McClean, G. Parr, and C. Grecos, "Analysis of coloured noise in received signal strength using the Allan Variance," in *22nd European Signal Processing Conference (EUSIPCO)*, 2014, pp. 994–998.

[42] C. Phillips and E. W. Anderson, "CRAWDAD data set cu/antenna (v. 2009-05-08)," Downloaded from http:// crawdad .cs .dartmouth .edu/cu/antenna, May 2009.

[43] S. Haykin, *Adaptive Filter Theory*. Pearson Education, 2014.

[44] J. Bendat and A. Piersol, *Random Data: Analysis and Measurement Procedures*, ser. Wiley Series in Probability and Statistics. John Wiley & Sons, 2010.

[45] P. Embrechts and M. Maejima, *Selfsimilar Processes*. Princeton, NJ, USA: Princeton University Press, 2002.

[46] S. M. Kay, *Fundamentals of Statistical Signal Processing. Estimation Theory*. Upper Saddle River, New Jersey (USA): Prentice–Hall, 1993.

[47] A. Sayed, A. Tarighat, and N. Khajehnouri, "Network-based wireless location: challenges faced in developing techniques for accurate wireless location information," *IEEE Signal Process. Mag.*, vol. 22, no. 4, pp. 24 – 40, July 2005.

[48] R. Malaney, "Nuisance parameters and location accuracy in log-normal fading models," *IEEE Trans. Wireless Commun.*, vol. 6, no. 3, pp. 937 –947, Mar. 2007.

[49] N. Patwari, J. Ash, S. Kyperountas, I. Hero, A.O., R. Moses, and N. Correal, "Locating the nodes: cooperative localization in wireless sensor networks," *IEEE Signal Process. Mag.*, vol. 22, no. 4, pp. 54 – 69, July 2005.

[50] J.-C. Chen, "Improved maximum likelihood location estimation accuracy in wireless sensor networks using the cross-entropy method," in *Acoustics, Speech and Signal Processing, 2009. ICASSP 2009. IEEE International Conference on*, Apr. 2009, pp. 1325 –1328.

Chunbo Luo is a Lecturer in Computer Science at the University of Exeter, UK. His research interests focus on developing model based and machine learning algorithms to solve networking and engineering problems such as wireless networks, unmanned aerial vehicles (UAVs) and computer vision. He received his PhD degree from the University of Reading, UK, for his work on the study of high performance cooperative wireless networks in 2011. He then joined the EPSRC SUAAVE project within the University of Ulster. He later took a Lecturer position at the University of the West of Scotland in 2013 and then moved to University of Exeter in 2015. He is a Fellow of the Higher Education Academy, an IEEE member and a BCS member. He is an invited reviewer of a group of IEEE Transactions, Elsevier journals and International Journal series.

Pablo Casaseca-de-la-Higuera received his MEng. in Telecommunications Engineering (2000) and his PhD in Information and Communication Technologies (2008) from the University of Valladolid (UVA), Spain. After working for three years in the aerospace Industry (Alcatel Espacio), he joined the Laboratory of Image Processing (LPI) at UVA in 2003 where he is currently an Associate Professor at the Department of Signal Theory & Communications, and Telematics Engineering. During 2013-2017 was appointed as a Lecturer (13-15) and Senior Lecturer (16-17) at the School of Engineering and Computing, University of the West of Scotland (UWS) where he is currently a visiting Senior Lecturer in Signal and Image Processing within the Artificial Intelligence, Visual Communication, and Networking research centre. He has published several book chapters and more than 60 papers in indexed journals and flagship international conferences. His research interests are signal and image processing and artificial intelligence with applications in biomedical engineering, computer vision, telecommunications, and unmanned aerial vehicles.

Sally McClean is Professor of Mathematics at Ulster University, which she joined after receiving an M.A. in Mathematics from Oxford University, a M.Sc. in Mathematical Statistics and Operational Research from Cardiff University and a Ph.D. in Mathematics (Stochastic Modelling) from the University of Ulster, She has over 350 publications, with research interests in Mathematical Modelling, Applied Probability, Multivariate Statistical Analysis, and applications to Healthcare and Computer Science, particularly database, telecommunications and sensor technology. She is Fellow of the Royal Statistical Society, Fellow of the Operational Research Society, Fellow of the Institute of Mathematics and its Applications and Member of the IEEE. In addition she is past president of the Irish Statistical Association and Leader of the Information and Communications Engineering Research group in Ulster Universitys Computer Science Research Institute.

Gerard Parr holds the Full Chair in Telecommunications Engineering and is Head of School of Computing Science at the University of East Anglia. He holds a PhD in Self Stabilising Protocols from Ulster University, aspects of which were completed with one of the founding Fathers of the Internet (Professor Jon Postel) as a Visiting Research Scientist at the DARPA/University of Southern California Information Sciences Institute in Marina Del Rey, Los Angeles. Within his academic career, areas of research include Wireless Sensor Clouds, Disaster Response Communications, Big Data event management, ICT for the Rural Economy, delay-sensitive protocols, and energy-aware autonomic networking for sensor-clouds and edge computing. He has advised governments on the allocation of funding to large-scale projects valued in total at approximately £2.5 billion.

Peng Ren received his BEng and MEng both in Electronic Engineering from Harbin Institute of Technology, China, and his PhD in Computer Science from the University of York, UK. He is currently a Professor with College of Information and Control Engineering, China University of Petroleum (East China). He received K. M. Scott Prize from the University of York in 2011, and was one coauthor of the Eduardo Caianiello Best Student Paper Award at 18th International Conference on Image Analysis and Processing (ICIAP) in 2015. He is a senior member of IEEE. His major interests include remote sensing and machine learning. He has published over academic 40 papers in these research fields.